Experimental study of a coupled thermo-hydraulic – neutronic stability of a natural circulation HPLWR

C. T'Joen, M. Rohde

Nuclear Engineering and Design, 242, 221-232, 2012

Experimental study of the coupled thermo-hydraulic - neutronic stability of a natural circulation HPLWR

C. T'Joen[1,2*], M. Rohde[1]

[1]Delft University of Technology, Department Radiation, Radionuclides & Reactors,

Mekelweg 15, 2629 JB Delft, The Netherlands

[2]Ghent University, Department of Flow, Heat and Combustion Mechanics,

Sint-Pietersnieuwstraat 41, 9000 Gent, Belgium

*corresponding author: c.g.a.tjoen@tudelft.nl, Tel: ++31152783811

Abstract

The HPLWR (High Performance Light Water Reactor) is the European concept design for a SCWR (SuperCritical Water Reactor). This unique reactor design consists of a three pass core with intermediate mixing plena. As the supercritical water passes through the core, it experiences a significant density reduction. This large change in density could be used as the driving force for natural circulation of the coolant, adding an inherent safety feature to this concept design. The idea of natural circulation has been explored in the past for boiling water reactors (BWR). From those studies, it is known that the different feedback mechanisms can trigger flow instabilities. These can be purely thermo-hydraulic (driven by the friction – mass flow rate or gravity – mass flow rate feedback of the system), or they can be coupled thermo-hydraulic - neutronic (driven by the coupling between friction, mass flow rate and power production). The goal of this study is to explore the stability of a natural circulation HPLWR considering the thermo-hydraulic - neutronic feedback. This was done through a unique experimental facility, DeLight, which is a scaled model of the HPLWR using Freon R23 as a scaling fluid. An artificial neutronic feedback was incorporated into the system based on the average measured density. To model the heat transfer dynamics in the rods, a simple first order model was used with a fixed time constant of 6 seconds. The results include the measurements of the varying decay ratio (DR) and frequency over a wide range of operating conditions. A clear instability zone was found within the stability plane, which seems to be similar to that of a BWR. Experimental data on the stability of a supercritical loop is rare in open literature, and these data could serve as an important benchmark tool for existing codes and models.

Keywords: supercritical fluid, stability, SCWR, neutronic feedback

Introduction

The SuperCritical Water Reactor (SCWR) is one of the six concept designs that is being studied as part of the international generation IV effort to develop more efficient, safer and proliferation resistant nuclear reactors, [1]. By raising the exit temperature the efficiency can be increased up to 42-45%, which is well above current reactors in operation. The use of supercritical water also results in a reduced complexity of the auxiliary systems and plant components, cutting investment costs, as highlighted by Buongiorno and Macdonald [2]. The idea of using supercritical water as a coolant matches the natural evolution for light water reactors (LWR), whereby pressure has increased from 7.5 MPa in boiling water reactors to 15.5 MPa in the current pressurized water reactors (PWRs). As such, this SCWR concept has already attracted a lot of interest and continues to do so. Over the course of the past decades a number of core designs have finalized, including a Japanese design [3], a Korean design [4], a US design [2] and most recently a European design [5]. These designs considerably differ in fuel assemblies, flow layout and moderators used. The European design (HPLWR, High Performance Light Water Reactor) [5] is remarkable as it contains a three-pass core layout (Fig. 1) combined with water rods for moderation. The system operates at 25 MPa, with an inlet and exit temperature of 280 °C and 500 °C respectively. Between the passes mixing plena are used to reduce peak cladding temperatures by homogenizing the flow into the passes. More details on the HPLWR fuel assembly can be found in [6]. The HPLWR has a thermal neutron spectrum, but core designs have also been presented for a fast (see e.g. [7]) and a mixed neutron spectrum ([8]). New modified designs are still being developed to tackle a range of issues, e.g. the SSCWR or Simplified SCWR ([9]) has a smaller core diameter but longer active length with axial enrichment variation. As a proof of concept, Vogt et al. [9] recently presented a concept using supercritical water in the primary loop as a first step in using supercritical water in a nuclear reactor with an exit temperature of 380 °C.

Also in the area of supercritical thermo-hydraulics a lot of research is being conducted. Because of the sharp variations of the fluid properties such as density near to the pseudo-critical point, the fluid behaviour is very complex due to combined effects of buoyancy and flow acceleration. A large number of experimental campaigns have been performed studying supercritical heat transfer, resulting in a large set of correlations, see e.g. [11]-[12] for reviews. However, when compared to experimental data, these correlations often show a very large scatter. New models and heat transfer deterioration criteria are being developed which include new non-dimensional numbers to quantify the buoyancy and flow acceleration (e.g. [13]-[14]). As such it is clear, that a lot of research is conducted into the reactor design (neutronics) and the fundamental thermo-hydraulics. Another important task is to design the entire power cycle, including the piping, turbines, and start up systems. Considering the large density difference that occurs over the reactor core, natural circulation could be considered as the driving force of the system. This removes the need for large feed water pumps, making the system more safe. Currently most reactor designs only consider natural circulation for emergency situations,

despite its inherent safety aspect. So far only one design, the ESBWR ([15]), has actually been constructed in a small size at Dodewaard, the Netherlands and was operated for decades. Currently, a number of (small size) reactors are under development with single phase natural circulation: e.g. the REX-10 (Regional Energy Reactor – 10 MW_{th}) which uses water at 2 MPa, [16]; the CHTR (Compact High Temperature Reactor – 100 kW_{th}) which uses a lead-bismuth eutectic mixture with temperatures up 1000 °C [17] and the CAREM 25 design (100 MW_{th}) which uses water at 12.25 MPa, [18]. Even though a lot of supercritical technology for the secondary side (such as turbines) already exists because of the fossil fuel based power plants, there still are large uncertainties with regards to corrosion and thermo-hydraulics of supercritical water in these tight lattice bundles; see e.g. [19]-[20].

Natural circulation loops however can become unstable under specific operational conditions (e.g. high power and low flow rate). Bouré et al. [21] and Durga Prasad et al. [22] presented a classification of the different types of instabilities and an overview of earlier work. A static instability (flow excursion, the so called Ledinegg instability) can be described using only the steady-state equations. In this case, a small change in the flow conditions will result in a new steady-state not in the vicinity of the original one. For dynamic instabilities, such as density wave oscillations or DWO, the steady-state equations are not sufficient to predict the system behavior, not even the threshold of instability. In such a situation, multiple competing solutions exist for the governing equations, and the system cannot settle down into anyone of them permanently. The system will move from one solution to the other, driven by feedback mechanisms. March-Leuba and Rey [23] presented a detailed explanation of the DWO and the feedback mechanisms, which is driven by the interaction of inertia and friction for the thermo-hydraulic modes. In a nuclear reactor another feedback mechanism is present: the neutronic feedback which couples the instant fluid density to the power production through the moderation. This results in a much more complex behavior, as shown by Van Bragt and Van der Hagen [24] for the ESBWR reactor and recently by Yi et al. [25] for the US design of a SCWR.

Most published results on the stability of supercritical flows are numerical and they consider either a forced single pass system ([26]-[29]) or an idealized loop geometry (e.g. [30]-[32]). These results were obtained using different codes which apply various techniques to study the stability (such as an eigenvalue analysis or transient simulations). Experimental data on natural circulation supercritical loops is rare in open literature, and as such, validation of these codes is difficult. For a single-pass, Ambrosini and Sharabi [28] compared three different methods to determine the stability boundary. Based on the good agreement between these methods and their diversity, they concluded their results were physically correct. Lomperski et al. [33] performed an experimental study on a rectangular supercritical CO_2 loop . They reported steady-state data and were unable to find any instabilities within the considered range. These findings did not agree with the accompanying numerical work by Jain [34], who did find a stability boundary at much lower powers.

The goal of this study is to examine the stability boundary of a naturally circulating HPLWR experimentally. To this end a setup has been designed and built, based on scaling analysis that will be briefly described further on. Neutronic feedback has been implemented artificially, and the time delay between the power production and the wall heat flux has been modeled using a single time constant. In the subsequent paragraphs the measurement setup and procedure will be described first before presenting the results. Because of the scarcity of experimental data on the stability of a supercritical loop in open literature, these data could serve as an important benchmark tool for existing codes and models.

Experimental setup: DeLight

To study the stability of a natural circulation driven HPLWR experimentally, a test facility must be designed. To reduce the pressure and temperature level and the power requirements imposed by the supercritical water to more suitable lab values, a scaling fluid was used. To design a scaled version of the HPLWR, the governing equations of the system should first be considered and made non-dimensional. Such can be done by selecting a reference state (the pseudo-critical point). The corresponding property data is listed in Table 1. Rohde et al. [35] describe the scaling procedure and derive a number of scaling factors based on the selected scaling fluid and the conservation of the Froude number and the friction distribution. It was shown that the friction distribution, rather than the actual value determines the linear stability behaviour. A friction scaling factor was then selected to allow for a large tube diameter, while preserving a large operational area. After comparison of a large number of different fluids, Freon R23 (CHF_3) was selected as the scaling fluid based on the power requirement, the temperatures (the pseudo-critical temperature is 33 °C), the pressure (5.7 MPa) and safety (non flammable). The non-dimensional fluid properties agree well, with a maximum deviation of 8% for the density far away from the pseudo-critical point . Through linear stability analysis of a channel with supercritical water and of its scaled R23 counterpart, it was shown that the scaling rules result in the same stability behaviour, confirming the proposed scaling procedure and fluid selection (see Rohde et al. [35]). This finding was also highlighted by Ambrosini [27], who found a very strong agreement between the stability boundary for different supercritical fluids provided the scaling was done correctly.

Based on the derived scaling rules, an experimental facility has been constructed at the Delft University of Technology, named ‘DeLight’ (Delft Light water reactor facility). A schematic drawing is shown in Fig. 2. The loop is constructed of stainless steel tubing (6 mm ID for the heating sections, 10 mm ID for the riser and downcomer). The total height of the loop is 10 m, which was derived from a preliminary force balance to ensure sufficient mass flow during all operating conditions. A complete description of the loop geometry can be found online, [36]. Up to 18 kW of heating (twice the nominal scaled power requirement) can be added in 4 tube sections (3 heating sections and the moderator

channel which mimics the water rod presence). Heating is done electrically (providing a uniform heat flux boundary) by sending a current through the tubes (up to 600 A per heating section using Delta SM15-200 power units). This results in a uniform heat flux imposed over the tube length. As such, the axial variation of the heat flux which naturally occurs in a reactor is not taken into consideration here and should be studied in the future. The power rating of each heating section can be set individually, as the power distribution per pass in the HPLWR core is non uniform. The first part of the core or evaporator accounts for 53% of the power production, the second one (superheater I) for 30% and the final heating section (superheater II) for 17%, see Fischer et al. [5]. Each heating section is electrically insulated from the other parts of the setup by using PEEK rings mounted in between two flanges. Valves are mounted at the inlet, exit and in between the heating sections, as well as at the exit of the riser. These valves can be used to introduce local friction in the system, such as inlet systems or the plena mimicking the actual HPLWR design. It is well known that local frictions such as orifices can have a significant effect on the stability of a supercritical system, see e.g. [28]-[29]. In this study, these valves are left open.

To provide a stable pressure level, a buffer vessel is present at the top of the loop with a moveable piston (Parker Series 5000 Piston Accumulator) connected to a nitrogen gas cylinder. By positioning this piston higher or lower the pressure level in the loop can be set at 5.7 MPa. Two heat exchangers (HX in Fig. 2) are mounted in series at the top section of the loop to extract the heating power and to set the inlet conditions. The first one uses cooling water (0.5 l/s) and cools R23 to 17 °C. The second one is an evaporator with R507a in which R23 is cooled down to a minimum temperature of -38 °C. Controlling the saturation pressure on the secondary side sets this temperature. Due to the differential thermal expansion of the heating sections (wall temperatures can reach over 200 °C) and the other parts of the loop, the tubes are connected to the wall using moveable spacers that contain two pre-stressed springs. The bottom connection between the different heating sections is made from a flexible tube of woven steel to allow for differential expansion.

The loop contains a large number of sensors. At the top and bottom absolute pressure sensors are presents (p symbol in Fig. 2, ± 0.15%). Each valve is combined with a differential pressure drop sensor (Δp symbol in Fig. 2, ±0.5%, ±200/500 mbar). The different heating sections each contain 5 type K thermocouples to measure the local fluid temperature as it passes through them (T symbol in Fig. 2, ± 0.1 K). These thermocouples also have to be insulated electrically from the tube to prevent the feed current passing through them. This was also done using PEEK rings. The individual thermocouple channels were carefully calibrated using 3 reference thermocouples that were calibrated over the entire temperature range by a certified body. As shown in Fig. 2 additional thermocouples are placed in the riser and downcomer section, as well as on the secondary side of the heat exchangers to monitor the heat removal. A number of capacitance sensors are present in the loop to monitor the local

density, indicated by a ‘C’ symbol in Figure 2. The R23 mass flow rate is measured using a coriolis meter (F symbol in Fig. 2, ± 0.25%, including a density measurement: ±0.005 kg/m³). Apart from the heating sections the entire setup is insulated using Armacell© (25 mm thick) to reduce any heat loss/gain to/from the environment. A magnetic rotor pump is present in the loop, but a bypass can be set to allow for natural circulation, as shown in Fig. 2.

The data acquisition system consists of a PC with one National Instruments PCI-6259 data acquisition card, connected to a National Instruments SCXI-1001 rack with two SCXI-1102B 32-channel amplifiers. This system is used for monitoring the experimental setup and for recording sensor signals. The measured and processed data are displayed, which allows for continuous monitoring. Up to 64 multiplexed signals are recorded for further analysis. Additionally, seven signals (three temperature values, two pressure values, and the R23 and cooling water flow rates) are connected to a separate stand-alone data acquisition system with a National Instruments NI-6035 DAQ card. This system is used for safety monitoring and will shut down the power supplies if one of the signals exceeds prescribed limits. A third PC is used to control the setup, setting the pressure level and the power input.

In order to mimic the behaviour of a nuclear reactor, neutronic feedback has to be included within the setup. This feedback mimics the effect of the water, whereby an increase of the density raises the moderating effect and thus increases the probability of fission, raising the power level. This is described through the reactivity $\Re$ of the system. The artificial feedback is based on a system developed by Kok and Van der Hagen [37] that was also used in a scaled boiling water system ([15]). Note that this only considers the density feedback, and not the temperature feedback (Doppler effect). The system is implemented by measuring the average core density $\bar{\rho}$ with the help of the 15 installed thermocouples and the equation of state for the density. To allow for a fast computation of the feedback, the equation of state was implemented as a series of splines $\rho = f(T)$, thereby neglecting the effect of the minimal pressure changes in the system. The node points for the splines were carefully selected and spaced more closely near to the pseudo-critical point. The maximum deviation of the spline sets compared to test data generated by the NIST database v.8 [38] on a fine grid of 0.01 °C was 0.9 % indicating a good accuracy of the splines. The measured density values are averaged over a sufficient time to determine the steady-state value $\bar{\rho}$. Once the neutronic feedback is engaged, the measured density variations are then used to calculate the reactivity via $\Re = r_\rho(\rho(t) - \bar{\rho})$. The change in power due to the reactivity feedback is calculated with the help of a linearized six-group, point-kinetic model. The point-kinetics equations can be found in reactor physics handbooks, e.g. [39]:

$$\frac{dn}{dt} = \frac{\Re - \beta}{\Lambda_{gen}} n(t) + \sum_{i=1}^{6} \lambda_i C_i(t) \qquad (1)$$

$$\frac{dC_i}{dt} = \frac{\beta_i}{\Lambda_{gen}} n(t) - \lambda_i C_i(t) \tag{2}$$

The precursor decay constants and fractions can be found in Table 2 and the delayed neutron faction β was set to 0.0056. These values were obtained from [40], but because of the time scaling in the facility, the decay constants need to be divided by the time scaling factor 0.438 ([35]). The mean generation Λ_{gen} was set to 22 μs, this is the scaled equivalent of a BWR value, [15]. The 6 group point-kinetics model was also used in [15], [25] and [40] to describe the neutronics in their coupled thermo-hydraulic – neutronic stability study. The fission rate and, subsequently, the heat generated in a reactor core by these fission reactions are directly correlated to the thermal neutron density, $n(t)$. The instantaneous volumetric heat generation in the fuel is given by:

$$q''' = w_f \Sigma_f n(t) v_n \tag{3}$$

The neutron density, the precursor concentrations and the reactivity can be expressed in terms of a steady-state value (e.g. $\bar{n}$) and a perturbation (e.g. n'). The point-kinetic equations (1)-(2) can then be rewritten in terms of these perturbations and linearized. By using Eq. (3), it then becomes clear that the resulting perturbation in the volumetric heating rate is directly proportional to the perturbation of the neutron density, n', and as such it is possible to recast the equations to describe the relative change to the original steady-state using $\underline{n}' \equiv \frac{n'}{\bar{n}}$:

$$\frac{d\underline{n}'}{dt} = \frac{\Re}{\Lambda_{gen}} + \left(\frac{\Re - \beta}{\Lambda_{gen}} \right) \underline{n}' + \sum_{i=1}^{6} \lambda_i \underline{C}_i'(t) \tag{4}$$

$$\frac{d\underline{C}'_i}{dt} = \frac{\beta_i}{\Lambda_{gen}} \underline{n}'(t) - \lambda_i \underline{C}_i'(t) \tag{5}$$

To make use of these equations the coupling between the reactivity and the density is required. The density feedback coefficient r_ρ is defined based on the work of Schlagenhaufer et al. [41] who studied the density feedback in the HPLWR. He presented a number of equations for different types of control rods. We considered the equation for withdrawn control rods in this work. As the density feedback coefficients presented by Schlagenhaufer et al. [41] also depend on the density, this would result in a varying density feedback at different points in the operational plane. In order to decouple the impact of the density feedback coefficient and other parameters that can affect stability (such as the fuel time constant), it was chosen to first implement a fixed value. This value $r_{\rho,DeLight}$ was set to 3.526 10^{-5} dk/k/(kg/m³), which is based on the average core density at nominal HPLWR operating conditions. This value 3.526 10^{-5} dk/k/(kg/m³) is already scaled to be used in the DeLight facility. In their study, Van Bragt and van der Hagen [24] also used constant feedback coefficients. Note that for a BWR it is

common to use the term ‘void’ reactivity feedback, which models the impact of the created void on the power, whereas in the SCWR the ‘density’ feedback is used. As a result the sign is different: : *increasing* void fraction in a BWR must result in a negative reactivity, whereas in an SCWR, a negative reactivity is achieved by a *decreasing* density.”

Using Eqs. (4)-(5) combined with the density feedback coefficient, it is possible to determine the change in volumetric heating rate required to mimic reactor behavior, based on the measured instantaneous density variation compared to the reference density. This computation is very fast, and as such using these equations would result in near instantaneous variation of the power input. In reality however, there is a time delay between the release of the fission energy within the fuel pellet and the moment when the coolant is exposed to the change in heat flux. This is because of the finite size of the fuel rod and the thermal conductivity. The time constant was set to 6 seconds, which is based on earlier experimental work on the ESBWR fuel rods ([42]). Note, that this value of 6 seconds isthen scaled in the DeLight setup, by multiplying it with 0.438, to account for the time-scaling ([35]). The precise value of the fuel time constant is related to the actual size of the fuel rod and the gap, and as such it can vary significantly, being as low as 2 seconds ([42]-[43]). Van Bragt and Van der Hagen [24] studied BWR stability and noted that the impact of the time constant is different for type I and type II instabilities: large fuel time constants have a stabilizing effect on Type-II oscillations, but the opposite effect on Type-I oscillations. Therefore, in a follow up study, the effect of the time constant should be examined. Using the Z-transformation, [44], a discretised equation (Eq. (6)) was obtained that could be implemented to determine the additional volumetric heat rate due to feedback $q'''^{n}_{feedback}$ at time n, based on the value at the previous time step and the value if no time delay would occur q'''^{n}. Here τ stands for the scaled fuel time constant.

$$q'''^{n}_{feedback} = \frac{1}{1+\frac{\tau}{\Delta t}}\left(q'''^{n} + \frac{\tau}{\Delta t} q'''^{n-1}_{feedback} \right) \tag{6}$$

Experimental procedure and data reduction

To experimentally determine the stability behaviour, the following procedure was used. First, the pump was used to start the circulation in the loop and a small amount of heating was added (1.5 kW). The pump was then switched off and bypassed, resulting in a naturally circulating fluid. The pressure was then raised above the critical pressure and the cooling setup was turned on. By simultaneously controlling the position of the piston and slowly incrementing the added heat, the system was brought to the required testing conditions (5.7 MPa, and a specified power input in the HPLWR distribution). To control the inlet temperature, the expansion pressure on the secondary side of HX2 was set manually. This was used to set levels such as -38 °C, -30 °C, -20 °C… To reach values in between or

for finer control of the inlet temperature, the moderator section at the bottom of the downcomer (see Fig. 2) was used. By adding more or less heat to this section, the temperature could be controlled to within 0.2 °C, and this was used to set intermediate inlet temperatures. To judge whether or not the system was stable, a number of signals were monitored: core inlet and outlet and heat exchanger outlet temperature (variation < 0.2 °C), and the absolute pressure variations in the loop (< 0.025 MPa).

Once a steady-state situation has been reached, the measurement was started. First over a period of 2 minutes the average core density is recorded. Then the neutronic feedback would be switched on, calculating the power corrections based on the measured instantaneous density and the stored average density (see equations above). If the system is unstable, the neutronic feedback will make the power input fluctuate with a growing amplitude. To prevent large pressure fluctuations in the loop, a limit was set on the fluctuation amplitude, constraining this to maximum 10% of the initial power. For an unstable system, the signals would then be recorded until this saturation is reached. If the system was stable, and no large oscillations were present two minutes after switching on the feedback, a step increase in the power (250 or 500 W) was done for 5 seconds. The decaying signal was then recorded until it was no longer distinguishable. Once the measurement was completed the power was raised by 250 W and the next point was recorded. This was continued until the DR values were no longer measurable (very stable system) or the core exit temperature exceeded 110°C (safety limit). The instabilities could be seen in all the recorded signals but they were most apparent in the temperature signals (e.g. at the inlet of the riser). To determine which signals were the most appropriate to use, a number of test cases were ran with a sinusoidal varying power input. The following signals were considered:

- Inlet temperature of the riser (thermocouple measurement)
- Mass flow rate through the loop (coriolis type mass flow meter)
- Local pressure drop over the exit valve of the core (differential pressure drop)

By using Fourier analysis it was found that all signals contained the main driving frequency of the varying power input, but that it was easiest to distinguish this frequency with a good accuracy from the temperature and pressure drop measurement. This suggests that the coupling between the frequency of the power input and the resulting mass flow rate is not that strong, which is probably due to the large buffer vessels in the loop (heat exchanger interior volume >> loop volume). So it was decided to use the inlet temperature signal of the riser as input for the signal analysis. Two examples of this measured temperature are shown in Fig. 3.

These temperature signals were then processed using signal analysis tools. All the sensor signals are sampled with a frequency of 120 Hz and then resampled to 20 Hz. Before resampling, the signals are filtered with a cut-off frequency of 9 Hz (Nyquist theorem). This was done using a digital filter

implemented in Matlab©. The resampling was done by taking a running average of 6 samples. These resampled data values were then used to determine the decay ratio 'DR'. This was done by fitting the equation $y = (1 - c_1 - a_1)e^{b_1 t} + c_1 + a_2 e^{b_2 t} \cos \omega t$ to the first two periods of the auto correlation function (ACF) of the signal. A similar function was used by Marcel, [45]. The DR is then defined by Eq. (7). As an extra check for the resonance frequency $f = \frac{\omega}{2\pi}$, the auto power spectral density is also determined, verifying it contains a single well defined peak at the frequency f. In the following section the measured DR values and response frequency f will be presented as contour plots (color coded). These plots were determined based on the individual set of measured data through interpolation on a cartesian mesh using Matlab. This was done in order to provide cleaner overview graphs of the stability plane rather than just show the individual data series. The individual measured data points can be obtained online [36]. Additionally an in depth uncertainty analysis will be presented.

$$DR = e^{\frac{2 \cdot \pi \cdot b_2}{|\omega|}} \tag{7}$$

Results

In order to represent the results in a more general form, a set of non-dimensional numbers are required. Because previous studies have used different formulations of the 1D transport equations, different non-dimensional units were derived to show the results. These numbers are mostly inspired by the earlier work done on boiling systems, seeking to extend the concept of the subcooling number and the phase change number into the supercritical range, as can be read in Ortega Gómez et al. [26] and Ambrosini and Sharabi [28]. Marcel et al. [46] proposed a scaling procedure to preserve the stability behavior of a supercritical loop. They suggested the pseudo phase change number N_{PCH} (Eq. (8)) and used the conditions at the inlet of the tube as reference values. This procedure was later modified by Rohde et al. [35] to include friction scaling. They also used the pseudo phase change number and defined a subcooling number (Eq. (9)), but suggested to use the pseudo-critical values as reference. The pseudo-critical enthalpy that was used as reference value is 288.03 kJ/kg.

$$N_{PCH} = \frac{q'' \cdot P_h \cdot L}{G_{in} \cdot A \cdot h_{ref}} \tag{8}$$

$$N_{SUB} = \frac{\left(h_{pc} - h_{in}\right)}{h_{pc}} \tag{9}$$

Steady-state power to flow map

Figure 4 shows three power flow curves measured with the DeLight facility at various inlet temperatures. As can be seen there is some scatter in the series, which is due to small temperature and

pressure variations between the individual data points. For each shown series, the inlet temperature is kept constant between ± 0.5 °C. As can be seen, these series show the expected trend: as the power increases, first the flow rate increases as well. This is due to the increased density difference that is the driving force for natural circulation. Starting from a given power the flow rate begins to decrease again. This is due to the increasing friction within the loop, which increases sharply as the velocity rises (decreasing density). Furthermore, increasing the inlet subcooling relative to the pseudo-critical point increases the flow rate, and shifts the maximum flow rate to a higher power. This is due to the density profile that occurs in the loop. By increasing the subcooling at the inlet, the inlet density rises, requiring thus a larger amount of heating in order to make it sufficiently low so that friction can balance the increased driving force. Note how the slope of the second half of the power flow curve becomes steeper at increased subcooling. These trends are all consistent with the published numerical work on supercritical loops [30]-[32]. As the temperature approaches the pseudo-critical point (33.1°C), there is a strong drop in the driving force, resulting in a lower flow rate.

Linear stability

There are two different types of DWO instabilities, labeled type I and type II, which can occur in a natural circulation loop. Type I instabilities are related to the gravitational pressure drop and occur for low steam qualities (~ low power), while type II instabilities are caused by the interplay of single and two-phase pressure drop. These thus occur mainly at high power. Both types can be purely thermo-hydraulic or coupled thermo-hydraulic – neutronic. During the experiments, no thermo-hydraulic instabilities (i.e. without neutronic feedback) were found in the considered power range. Switching on the neutronic feedback did result in the occurrence of instabilities. As such, all the shown data shown below is for the coupled neutronic – thermo-hydraulic instability. This is consistent with earlier work: Van Bragt and van der Hagen [24] showed that for a natural circulation BWR the coupled neutronic – thermo-hydraulic mode is less stable than the pure thermo-hydraulic mode, shifting the stability ‘peak’ to the left in the stability plane. They also showed that for the coupled neutronic – thermo-hydraulic mode, the ‘peak’ in the stability region becomes much more narrow and extends up to higher N_{SUB}. Similar findings were reported by Yi et al. [25] for a forced SCWR. Ortega-Gomez [40] also found that for a single channel with supercritical water at low N_{SUB} the coupled neutronic – thermo-hydraulic mode is less stable than the pure thermo-hydraulic mode. However, the absence of pure thermo-hydraulic instabilities up to higher powers (as indicated by the measurements), suggests that there is a very significant difference between these two instability modes for the considered system. A possible cause for the suppression of the thermo-hydraulic instabilities is the large interior volume of the heat exchangers ($7.5\ 10^{-3}\ m^3$) compared to that of the loop (roughly $2\ 10^{-3}\ m^3$). The heat exchangers can thus act as strong dampers to perturbations.

A total number of 338 points was measured with an inlet temperature varying between -29.7 °C and 19.3 °C. The power ranged between 2 and 9.3 kW. The resulting contour plot of the DR values can be seen in Fig. 5. The black line indicates DR = 1, the neutral stability line. As can be seen, for a given inlet temperature (N_{SUB} = constant) the system undergoes two transitions. At low power, the system is stable (DR < 1), and raising the power results in increasing DR values until the system eventually crosses the stability boundary and becomes unstable. Continuing to increase the power makes the DR decrease again until the system is stable again. As such the DR shows a maximum. Jain and Uddin [30] and Jain and Corradini [32] did not report this behavior, which could be because they only searched for the first transition by incrementing the power from a low value. This maximum behaviour was also found by Sharma et al. [31] who studied a rectangular supercritical loop with water at 25 MPa. They also noted that above a certain inlet temperature no instabilities occur, which was also found here. For an $N_{SUB} < 0.18$ there is no instability. This could therefore be considered as a safe zone for operation. However, at these high inlet temperatures, the flow rate that can be achieved is rather low and this could limit the heat transfer to the coolant, imposing a power constraint on the reactor. This could be an interesting design idea for new natural circulation reactors.

The presented stability map is similar to the ones that have been reported for a natural circulation driven BWR, see Fig. 6 which is reproduced from Van Bragt and Van der Hagen [24]. In such a system, for a given subcooling number, the flow will undergo three transitions: (i) from stable to unstable, thereby crossing the boiling line $h_{out} = h_{sat}$ (indicated by the dashed line) and moving towards the low frequency type-I instability, (ii) from unstable to stable and (iii) then, at higher powers, again from stable to unstable, thereby crossing the neutral stability line and moving towards the high frequency type-II instability. From the experiments, there is a strong evidence that the first two transitions related to BWRs are found in natural circulation driven supercritical systems as well: (i) from stable to unstable, thereby crossing the left branch of the neutral stability line. This left branch is equivalent to the boiling line of BWR's, but is less sharply defined, as there is no such clear distinction between 'boiling' and 'non-boiling' for a supercritical fluid; and (ii) from unstable to stable, thereby crossing the right branch of the neutral stability line. In Figs. 5, 7 and 8 the supercritical equivalent of the boiling line, the 'reference line', $h_{out} = h_{pc}$ is shown as a black dashed line to highlight the equivalent behavior between both systems. For a boiling system if $T_{out} < T_{sat}$ (= reference value), no boiling occurs and as such there is no void fraction to trigger instabilities, see Fig. 6. But as the density of a supercritical fluid is a continuous function, it should be clear that even if the temperature at the outlet is lower than T_{pc} (= reference value), a strong density gradient can occur, which can trigger instabilities. This in fact has been shown here experimentally, as the unstable zone crosses the reference line around $N_{SUB} = 0.25$ and then moves almost parallel to it at higher N_{SUB} values. This trend suggests that above $N_{SUB} = 0.27$ an exit

temperature close to T_{pc} could be used as a criterion for instability. The graphs reported by Sharma et al. [31] show a similar trend for the thermo-hydraulic mode, whereby the first instability threshold is constant at a temperature near to T_{pc}, but it was not mentioned if this value is above or below it. Sharma et al. [31] also showed that this first transition is insensitive to the loop height and local friction distribution (though only small variations were examined). This indicates that this boundary is a more general property of a supercritical loop, which is consistent with the aforementioned idea of extending the reference line from type I instabilities of BWR.

In the unstable region, the frequencies are found to be low, i.e. the period of the oscillations corresponds well with the traveling time of the fluid through the core and riser sections (~0.25 Hz, see Fig. 7). Such low frequencies are typically related to gravity-driven type-I instabilities. The high frequencies that are expected at higher powers, however, were not found in the experimental campaign due to safety constraints. The numerous studies on (natural circulation driven) BWR and forced-circulation SCWR stability ([28], [40]), all show that the neutral stability line has a negative slope for increasing N_{PCH}. We therefore expect that, similar to natural circulation driven BWR's, there should be a third transition towards type-II instabilities. Further study is required to confirm the occurrence of such a transition. An interesting finding is that there exists a trajectory to move from zero power/low inlet temperatures towards high power/high inlet temperatures without crossing a stability threshold, something that is impossible for natural circulation BWR's as the boiling boundary and the neutral stability boundary cross each other at the origin of the stability plane. Such a power trajectory might be exploited during the start-up phase of the HPLWR as long as the reactor vessel can be pressurized beforehand.

Figure 5 also clearly illustrates how close to the low power stability threshold, the DR value suddenly increases sharply. This is also illustrated below in the section on measurement qualification where individual DR value plots are shown for a single N_{SUB}. A small change in operational parameters (a few % only), can result in a significant change of the DR value. The same is true for the frequencies, as shown in Fig. 6. This was also found by Van der Hagen et al. [47] when performing experiments on the actual Dodewaard reactor (natural circulation) and by Yi et al. [25] for a forced circulation SCWR.

Figure 8 shows the contour plot of the measured mass flow rates, also indicating the zone of instability (black line) and the reference line (black dashed line). Chatoorgoon [49] previously postulated that the onset of thermo-hydraulic instabilities in a supercritical loop was linked to the peak of the power flow-to-map: $\frac{\partial M}{\partial P} = 0$. For a simplified loop case he was able to show good agreement between this criterion and his own numerical code. However, Jain and Uddin [30] later showed that the results of Chatoorgoon [49] were not independent of the time step or the spatial

discretisation. By using smaller time steps and a finer grid, Jain and Uddin [30] obtained a converged solution that showed a transition to instability before the mass flow peak is reached. Sharma et al. [31] reported the ratio of the power of the first stability threshold to the power corresponding to the peak steady-state mass flow rate, and they too showed that this value is different from 1. They reported that the value was smaller than 1 for large subcooling, but as the subcooling decreases the value becomes larger than 1, indicating the flow is stable into the friction dominated regime for thermo-hydraulic modes. As no thermo-hydraulic instabilities were found, this loop system is stable well into the friction regime, as shown by Fig. 4. Furthermore, the results of Fig. 5 indicate that the first threshold of instability for the coupled neutronic – thermo-hydraulic mode in this system always occurs before the maximum mass flow rate for the range of N_{SUB} studied here (qualitatively indicated by the white dashed line).

Frequency map

Figure 7 shows the corresponding contour plot of the fitted frequencies. The solid black line for DR = 1 and the dashed reference line are also indicated. As can be seen, the overall trend is very similar to that of the DR value contour plot, whereby the frequencies show a maximum at the centre of the unstable zone. The measured frequencies are in the order of 0.2 Hz near the transitions, which is comparable to that of type I instabilities in a BWR, [15], [24]. This again indicates the similarity between these instabilities and those in a BWR. Jain and Uddin [30] did not report the frequency of their instability, but from a time dependent graph in their paper a value of 0.15 Hz can be determined, which is very close to the measured values here. Yi et al. [25] reported a value of about 0.3 Hz, and also found that near the stability threshold, the frequency increased fast. Sharma et al. [31] did not report any frequency information in their paper.

Non linear behaviour

Non-linear behaviour in natural circulation systems is of interest because under abnormal operating conditions such as a reactor trip or a loss of coolant accident, the perturbations in the system are so large that linear stability no longer applies to capture the physics of the system. The effects of nonlinearities can amplify and the system may suddenly jump to new region (e.g. a limit cycle) far away from the original state. This makes it a dangerous situation for real reactors, and a highly investigated topic, see e.g. Durga Prasad et al. [22] for a review of earlier work. Different researchers have successfully used nonlinear dynamics (such as bifurcation analysis and chaos theory) to study the system behaviour under wide operating conditions and for large parametric fluctuations, e.g. Van Bragt and Van der Hagen [24]. During the measurement campaign a number of measurements clearly showed non-linear behaviour. These were all located in the proximity of the stability thresholds. Figure 9 shows an example of a so called limit cycle, close to the first

stability threshold. Upon activating the neutronic feedback the perturbations start to grow, but then from a certain moment the growth decreases and a constant oscillation would be sustained for a long period of time.

Uncertainty analysis and measurement qualification

In order to assess the quality of the measurements, a thorough error analysis was performed. This includes a careful estimate of the different uncertainty contributions as well as a thorough validation of the fitting procedure that was used. The reproducibility of the results was also verified. Standard error propagation rules as described by Taylor [50] were used to determine the total uncertainty on e.g. N_{PCH}. An uncertainty of 2% was assumed on h_{pc}. In order to better qualify the measurement procedure, it was verified that the used steering frequency or the use of preheating with the moderator section did not affect the results.

Fitting uncertainty

As stated above, the reported DR values and frequency are determined based on fitting the equation $y = (1 - c_1 - a_1)e^{b_1 t} + c_1 + a_2 e^{b_2 t} \cos \omega t$ to the first two periods of the auto correlation function of the resampled temperature signal. This was done through the *nlinfit* module of Matlab© which provides the coefficient estimates, the resulting residuals and an estimated coefficient covariance matrix. These values can then be used in the *nlparci* module to determine the 95% confidence intervals for the estimated coefficients. These values were then used in an error propagation to determine the uncertainty on DR and f due to fitting, δDR_{fit}. The fit itself is illustrated in Fig. 10. As can be seen the agreement is very well, and this was the case for most measured points, provided the DR was higher than 0.5 and smaller than 2.5. This is because a sufficient number of oscillation periods are needed in the recorded temperature signal. If the DR value is below 0.5 it decays too fast into the background oscillations of the loop, and if the DR value is above 2.5, the signal saturates too fast due to the imposed power limit. The resulting average uncertainties are very small: 0.6% in the considered range. Using this type of autocorrelation fit to determine the decay ratio of a measured signal has been shown to be accurate over a wide range of DR values in BWR, [51].

During the fitting procedure a time window has to be selected over which the fitting is done. In order to further validate the fitting procedure, the effect of this window selection was investigated on 25 signals that had a DR value close to 1. As such they could be measured for a long time without fading out or resulting in saturation. These signals were divided into different time windows and the fitting analysis was done on each window individually. The resulting DR value and frequencies were then compared. An example is shown in Fig 11. Figure 11 A shows the actual recorded signal and the considered windows, which also varied in size. Fig 11 B shows the resulting measured DR values. As

can be seen, there are small differences between the fitted values, but most values agree to within the fitting uncertainty. The average of the different values is indicated with the dashed line. The resulting scatter for the frequency values was similar. The results show that short windows are slightly less accurate and therefore, always the largest possible window considering the recorded data was selected. The same trend was found for the fitted frequencies.

It should be noted that with the used fitting technique it is difficult to measure DR values smaller than 0.5 or larger than 2.4 accurately. This is because a sufficient number of oscillation periods are needed in the recorded temperature signal, and if the DR value is below 0.5 it decays too fast into the background oscillations of the loop. This is why the DR maps has a skewed look, as it was impossible to measure the DR accurately in the top left and bottom right corner of the stability plane.

Uncertainty due to temperature and pressure

The inlet temperature of the heating section can be controlled to within a variation of ±0.2 °C. During the measurements however, there can be a slight drift. This is because of slow variations that occur in the loop related to the natural circulation. Usually the exit temperature of heat exchanger 2 will vary within ±0.2 °C and the absolute pressure shows variations of ±0.025 MPa. Because the mass flow rate is not set, as it is driven by density differences, these small pressure and temperature fluctuations cause the flow rate to vary slightly. For a fixed power input (set for a measurement), this results in small temperature differences. As such, the DR values of individual measurements will differ slightly. It is important to assess how strong this effect is, in order to estimate the resulting uncertainty. This was done by searching the dataset for points which had the same power setting and slight differences in the absolute pressure and inlet temperature. Figure 12 shows a number of these points which are grouped per 2 or 3 (fixed power setting and inlet temperature) but which have slight pressure differences. These points cover a wide range of measured DR values (from 0.78 to 1.72). In Fig. 12 both the uncertainty on the pressure and the fitting uncertainty on the DR value are indicated. As can be seen, the values correspond quite well, but the differences between them are larger than the fitting uncertainties. So an additional uncertainty should be taken into account. The same conclusion was drawn when the temperature effect was examined. This was done by plotting data points with a same power setting and inlet pressure but moderate temperature variations. It is however difficult to show clearly in a graph because of the wide range of temperatures. Based on these two surveys, it was decided to add a conservative additional uncertainty related to the pressure and temperature effect of 0.05 to the DR value, independent of the pressure or temperature level. This value was then added to the fitting uncertainty as an independent variable to determine the total uncertainty:

$$\delta DR_{tot} = \sqrt{0.05^2 + \delta DR_{fit}^2} \quad (15)$$

Reproducibility

In order to verify that the measurements were reproducible, two data series with the same inlet condition (-17 °C) that were recorded on different days (separated by 3 weeks) were compared. The results can be seen in Fig. 13. It is clear that the two series match to within the uncertainty range. In this graph the DR values are shown with δDR_{tot} as uncertainty. Similarly, the frequency data was well reproducible.

Impact of the power steering frequency and the preheater

Because of the large amount of channels that is monitored (and of which the data is recorded) and the calculation time required to determine the neutronic feedback value, the feedback could only be implemented with a frequency of 20 Hz. It is important to assess that this frequency does not affect the final outcome. Therefore, this frequency was further lowered to 12 Hz and an earlier measured series was repeated. The results are shown in Fig. 14A. As can be seen, they correspond very well, indicating that this steering frequency has no effect on the results. In Fig. 14B the DR values are compared for 2 series with T_{in} = -17 °C. For one series this was achieved without using preheating through the moderator section, for the other one preheating was used (meaning the exit temperature of the heat exchanger was lower ~ -22 °C). As can be seen, there is no influence on the measured DR value, which is due to the short length of the preheater compared to the downcomer. Also the mass flow rate was the same, to within the measurement uncertainty. This makes sense, as the total change in driving force by adding a few degrees over a short distance at the end of the downcomer is negligible.

Core averaged density uncertainty

To perform the neutronic feedback, the core averaged density is required. This value is determined based on 15 temperature measurements (5 in each heating section). Because each of these temperature measurements has an uncertainty of ±0.2 °C, it was important to assess how large the uncertainty on the average density is based on these values. This was done using a 1D model, whereby the imposed wall heat flux and measured mass flow rate and inlet temperature are used as input. The enthalpy change can then be computed through the three sections (neglecting heat losses), which gives an exact value for the averaged density. For the 15 locations the local temperature can then be extracted from the density, but these values are then perturbed by ±0.2 °C and a new perturbed density value is determined. The average of these 15 perturbed values was then compared to the exact case. The resulting deviation was always smaller than 1.5%, and in most cases smaller than 0.5%. For a number

of data points, the measurement was repeated with a perturbed value for $\bar{\rho}$. The results showed that the DR and frequency were the same, but this could only be tested for low power values, because perturbing this value at higher powers resulted in large pressure changes, shifting the operational pressure away from 5.7 MPa. As such, we feel that the proposed method to evaluate the average water density for the neutronic feedback is sufficiently verified.

Conclusions

In this paper the stability of a scaled, experimental model of a natural circulation driven HPLWR has been examined. The decay ratio values and resonance frequencies have been measured for a range of operational conditions in terms of power and core inlet temperature. The experimental facility, named Delight, is a scaled version of the HPLWR, and uses Freon R23 at 5.7 MPa as a scaling fluid. In order to mimic a nuclear reactor, an artificial neutronic feedback was implemented based on a measurement of the average density and the 6 group point kinetics equations. Furthermore a model for the heat transfer within the fuel rod was also implemented, describing the heat transfer process through a single time constant τ. No thermo-hydraulic instabilities occurred at the considered power range, but a clear zone of instability was found within the operational plane for the coupled neutronic – thermo-hydraulic mode. This indicates that for a single core inlet temperature there exists a low and high power stability threshold, provided the N_{SUB} is higher than 0.18. Below this value, no instabilities were recorded. The location of these instabilities within the operational plane and the low frequency (~ 0.2 Hz) suggest, based on previous studies on natural circulation driven boiling water reactors, that these are the equivalent of type-I instabilities. Extending this analogy suggests that another transition to the high-frequency type-II instabilities will occur at high power levels, which were not accessible due to safety constraints.. In contrast to natural circulation BWR's, there exists a stable trajectory from zero-power/low inlet temperatures to high power/high inlet temperatures that can be exploited during the start-up phase of a natural circulation driven SCWR. Close to the stability thresholds, the DR value changes abruptly, which indicates that this value is insufficient as online monitor for reactor stability, more information is required. This issue has also been identified in BWRs, [48]. Finally, these data can serve as an important benchmark for computational tools, because data on supercritical loop stability is rare in open literature.

Acknowledgements

The authors would like to express gratitude to the Netherlands Organization for Scientific Research (NWO), project number 680-47-119 and to the EU FW7 THINS project, which provided support for the current study and thank Ing. D. de Haas and Ing. P. van der Baan for their technical expertise in designing and building the setup as well as setting up the data acquisition and analysis tools.

Nomenclature

A	cross sectional flow surface area [m^2]
C_i	delayed neutron precursor concentration [$1/m^3$]
C_j	local friction value (orifice)
D_h	hydraulic diameter [m]
DR	decay ratio [-]
f	Darcy Weisbach friction factor [-]
g	gravimetric acceleration [m/s^2]
G	mass flux [kg/m^2s]
h	enthalpy [J/kg]
L	length of the heater [m]
M	mass flow rate [kg/s]
n	neutron density
N_{PCH}	pseudo phase change number, Eq. (13) [-]
N_{SUB}	subcooling number, Eq. (14) [-]
p	static pressure [Pa]
P	power [W]
P_h	heated perimeter [m]
Δp	pressure drop [Pa]
q”	heat flux [W/m^2]
q’’’	volumetric heat input [W/m^3]
r_ρ	density coefficient of reactivity [$dk/k/(kg/m^3)$]
$\Re$	reactivity [-]
Δt	time step [s]
t	time [s]
T	temperature [°C]
v_n	neutron velocity [m/s]
w_f	energy released per fission event [J per event]

X	schaling factor
z	coordinate [m]

Greek symbols

β	delayed neutron fraction [-]
θ	angle relative to the horizontal axis, 0° in this study
λ_i	precursor decay constant of group i [1/s]
Λ_{gen}	mean generation time [s]
ρ	density [kg/m^3]
Σ_f	macroscopic cross section for fission [/m]
τ	fuel time constant [s]

Subscripts

feedback	due to feedback
in	inlet
out	outlet
pc	value at the pseudo-critical point
ref	value at the reference point
sat	value at the saturation point

References

[1]. U.S. DOE Nuclear Energy Research Advisory Committee and the Generation IV International Forum, A Technology Roadmap for Generation IV Nuclear Energy Systems, 2002, available online: http://gif.inel.gov/roadmap/pdfs/gen_iv_roadmap.pdf

[2]. Buongiorno J and MacDonald PE, Supercritical water reactor (SCWR), progress report for the FY-O3 Generation IV R&D activities for the development of the SCWR in the U.S., Report INEEL/EXT-03-01210, 38 pages, 2003.

[3]. Oka, Y., Koshizuka, S.I., 1993, Concept and Design of a Supercritical-Pressure, Direct-Cycle Light-Water Reactor, Nuclear Technology 103, 295-302

[4]. Bae, Y.-Y., Jang, J., Kim, H.-Y., Kang, H.-O., Bae, K.-M., 2007, Research activities on a supercritical water reactor in Korea, Nuclear Engineering and Technology 39, 273-286.

[5]. Fischer, K., Schulenberg, T., Laurien, E., 2009, Design of a supercritical water-cooled reactor with a three-pass core arrangement, Nuclear Engineering and Design 239, 800-812

[6]. Hofmeister, J., Waata, C., Starflinger, J., Schulenberg, T., Laurien, E., 2007, Fuel assembly design study for a reactor with supercritical water, Nuclear Engineering and Design 237, 1513-1521.

[7]. Oka, Y., Koshizuka, S.I., 2001, Supercritical-pressure, once-through cycle light-water cooled reactor concept, Journal of Nuclear Science and Technology 38, 1081-1089

[8]. Liu, X.J., Cheng, X., 2010, Coupled thermo-hydraulics and neutron-physics analysis of SCWR with mixed spectrum core, Progress in Nuclear Energy 52, 640-647.

[9]. Reiss, T., Csom, G., Fehér, S., Czifrus, Sz., 2010, The simplified supercritical water reactor (SSWCR), a new SCWR design, Progress in Nuclear Energy 52, 177-189

[10]. Vogt, B., Fischer, K., Starflinger, J., Laurien, E., Schulenberg, T., 2010, Concept of a pressurized water reactor cooled with supercritical water in the primary loop, Nuclear Engineering and Design 240, 2789-2799

[11]. Pioro, I.L., Khartabil, H.F., Duffey, R., 2004, Heat transfer to supercritical fluids flowing in channels – empirical correlations (survey), Nuclear Engineering and Design 230, 69-91.

[12]. Cheng, X., Schulenberg, T., 2001, Heat transfer at supercritical pressures – literature review and application to an HPLWR, FZKA6609, Forschungszentrum Karlsruhe GmBH, Karlsruhe, 47 pages

[13]. Jackson, J.D., 2011, A model of developing mixed convection heat transfer in vertical tubes to liquids at supercritical pressure, Proceedings of the 5th International Symposion on SCWRS, ISSCWR5, March 13-16, Vancouver, Canada.

[14]. McEligot, D.M., Jackson, J.D., 2004, "Deterioration" criteria for convective heat transfer in gas flow through non-circular ducts, Nuclear Engineering and Design 232, 327-333

[15]. Marcel, C.P., Rohde, M., Van der Hagen, T.H.J.J., 2008, Experimental investigations on the ESBWR stability performance, Nuclear Technology 25, 232-244

[16]. Jang, B.-I., Kim, M.H., Jeun, G., 2011, Experimental and computational investigation of a natural circulation system in Regional Energy Reactor – 10 MWth, Nuclear Engineering and Design 241, 2214-2223

[17]. Dulera, I.V., Sinha, R.K., 2008, High temperature reactors, Journal of Nuclear Materials 383, 183-188

[18]. Zanocco, P., Gimenez, M., Delmastro, D., 2004, Modeling aspects in linear stabiltiy analysis of a self-presurised, natural circulation integral reactor, Nuclear Engineering and Design 231, 283-301

[19]. Was G.S., Ampornrat, P., Gupta, G., Teysseyre, S., West, E.A., Allen T.R., Sridharan, K., Tan, L., Chen, Y., Ren, X., Picter, C., 2007, Corrosion and stress corrosion cracking in supercritical water, Journal of Nuclear Materials 371 (3), 176-201

[20]. Pentilla, S., Toivonen, A., Heikinheimo, L., Novotny, R., 2010, Corrosion studies of candidate materials for European HPLWR, Nuclear Technology 170, 261-271.

[21]. Bouré, J.A., Bergles, A.E., Tong, T.S., 1973, Review of two-phase flow instability, Nuclear Engineering and Design 25, 165-192

[22]. Durga Prasad, G.V., Pandey, M., Kalrat, S.M., 2007. Review of flow instabilities in natural circulation boiling water systems, Progress in Nuclear Energy 49, 429-451.

[23]. March-Leuba, J., Rey, J.M., 1993, Coupled thermohydraulic-neutronic instabilities in boiling water nuclear reactors: a review of the state of the art, Nuclear Engineering and Design 145, pp. 97-111

[24]. Van Bragt, D.D.B., T.H.J.J. van der Hagen, 1998, Stability of natural circulation boiling water reactors: part II: parametric study of coupled neutronic-thermohydraulic instabilities, Nuclear Technology 121, 52-62

[25]. Yi, T.T., Koschizuka, S., Oka, Y., 2004, A linear stability analysis of supercritical water reactors (II): coupled neutronic thermal-hydraulic instability, Journal of Nuclear Science and Technology 41, 1176-1186

[26]. T. Ortega Gómez, A. Class, R.L. Lahey Jr., T. Schulenberg, 2008, Stability analysis of a uniformly heated channel with supercritical water, Nuclear Engineering and Design 238, 1930-1939

[27]. Ambrosini, W., 2009, Discussion on the stability of heated channels with different fluids at supercritical pressures, Nuclear Engineering and Design 239, 2952-2963

[28]. Ambrosini, W., Sharabi, M., 2008, Dimensionless parameters in stability analysis of heated channels with fluids at supercritical pressures, Nuclear Engineering and Design 238, pp. 1917-1929

[29]. W. Ambrosini, 2007, On the analogies in the dynamic behavior of heated channels with boiling and supercritical fluids, Nuclear Engineering and Design 237, 1164-1174

[30]. P.K. Jain, R. Uddin, 2008, Numerical analysis of supercritical flow instabilities in a natural circulation loop, Nuclear Engineering and Design 238, 1947-1957.

[31]. Sharma, M., Pilkhwal, D.S., Vijayan, P.K., Saha, D., Sinha, R.K., 2010, Steady state and linear stability analysis of a supercritical water loop, Nuclear Engineering and Design 240, 588-59

[32]. R. Jain, M. Corradini, 2006, A linear stability analysis for natural circulation loops under supercritical conditions, Nuclear Technology 155, 312-323

[33]. Lomperski, S., Cho, D., Jain, R., Corradini, M.L., 2004, Stability of a natural circulation loop with a fluid heated through the thermodynamic pseudocritical point, Proceedings of ICAPP'04, Pittsburgh, PA, USA, June 13-17

[34]. Jain, R., 2005, Thermal-hydraulic instabilities in natural circulation flow loops under supercritical conditions, Ph.D. Thesis, University of Wisconsin Madison, USA

[35]. Rohde, M., Marcel, C.P., T'Joen C., Class, A., Van der Hagen, T.H.J.J., 2011, Downscaling a supercritical water loop for experimental studies on system stability, International Journal of Heat and Mass Transfer 54, pp. 65-74

[36]. DeLight webpage, http://tnw.tudelft.nl/en/about-faculty/departments/radiation-radionuclides-reactors/research/research-groups/physics-of-nuclear-reactors/facilities/delight/

[37]. Kok, H.V., Van der Hagen, T.H.J.J., 1999, Design of a simulated void-reactivity feedback in a boiling water loop, Nuclear Technology 128, 1-11

[38]. NIST REFPROP, reference fluid thermodynamic and transport properties, U.S. Department of Commerce, Washington DC (2007) NIST standard reference database 23, version 8.0

[39]. Duderstadt, J.J., Hamilton, L.J., Nuclear reactor analysis, John Wiley & Sons, 1976

[40]. Ortega-Gomez, T., 2009, Stability analysis of the High Performance Light Water Reactor, Ph.D. Thesis, Forschungszentrum Karlsruhe, Institute for nuclear and energy technologies, University of Karlsruhe

[41]. Schlagenhaufer, M., Vogt, B., Schulenberg, T., 2007, Reactivity control mechanisms for a HPLWR fuel assembly, Proceedings of Global 2007, 934-943, Boise, ID, USA, September 9–13.

[42]. Van der Hagen, T.H.J.J., 1988, Experimental and theoretical evidence for a short effective fuel time constant in a boiling water reactor, Nuclear Technology 83, 87-97

[43]. Van der Hagen, T.H.J.J., 1998, Fuel heat transfer modeling in reduced order boiling water reactor dynamic models, Annals of Nuclear Energy 25, 1287-1300.

[44]. Kam, F., 2011, Development of a one-dimensional computer model for the stability analysis of a natural circulation supercritical water reactor, Msc. Thesis, Delft University of Technology

[45]. Marcel, C.P., 2007, Experimental and Numerical Stability Investigations on natural Circulation Boiling Water Reactors, Ph.D. Thesis, Delft University of Technology

[46]. Marcel, C.P., Rohde, M., Masson, V.P., Van der Hagen, T.H.J.J., 2009, Fluid-to-fluid modeling of supercritical water loops for stability analysis, International Journal of Heat and Mass Transfer 52, 5046-5054

[47]. Van der Hagen, T.H.J.J., Van Bragt, D.D.B., Van der Kaa, F.J., Karuza, J., Killian, D., Nissen, W.H.M., Stekelenburg, A.J.C., Wouters, J.A.A., 1997. Exploring the Dodewaard type-I and type-II stability: from startup to shut down, from stable to unstable, Annals of Nuclear Energy 24, 659-669

[48]. Van der Hagen, T.H.J.J., Zboray, R., de Kruijf, W.J.M., 2000. Questioning the use of the decay ratio in BWR stability monitoring, Annals of Nuclear Energy 27, 727-732.

[49]. Chatoorgoon, V., 2001, Stability of supercritical fluid flow in a single channel natural convection loop, International Journal of Heat and Mass Transfer 44, 1963-1972

[50]. Taylor, J.R., 1997, An introduction to error analysis, 2nd ed, University Science Books, Sausalito

[51]. Manera, A., Zboray, R., Van der Hagen, T.H.J.J., 2003. Assessment of linear and non-linear auto-regressive methods for BWR stability monitoring, Progress in Nuclear Energy 43, 321-327

Figure Captions

Figure 1. Schematic representation of the HPLWR, reproduced from Fischer et al.[5].

Figure 2. Schematic of the DeLight facility indicating the location of the different sensors.

Figure 3. Examples of a stable (A) and unstable (B) temperature signal measured at the inlet of the riser section

Figure 4: Measured power flow map data for a few selected inlet temperatures, R23 at 5.7 MPa.

Figure 5. Contour plot of the measured DR values. The black line indicates DR = 1, the neutral stability line. The dashed line indicates where the exit temperature is equal to the pseudo-critical value.

Figure 6. BWR stability plot, reproduced from Van Bragt and Van der Hagen [24].

Figure 7. Contour plot of the measured frequencies. The black line indicates DR = 1, the neutral stability line. The dashed line indicates where the exit temperature is equal to the pseudo-critical value.

Figure 8. Contour plot of the measured mass flow rates (in g/s). The black line indicates DR = 1, the neutral stability line. The black dashed line indicates where the exit temperature is equal to the pseudo-critical value. The white dashed line qualitatively indicates the location of the maximum flow rate.

Figure 9. Illustration of non-linear effects which were recorded during the measurements: the occurrence of a limit cycle near the low power threshold.

Fig. 10. Illustration of the fitted function and the autocorrelation of the measured temperature signal, N_{SUB}: 0.4, N_{PCH}: 0.37.

Figure 11. Verification of the fitting procedure to determine DR values. A: measured time signal and the selected windows, B: fitted DR values with their fitting uncertainty, N_{SUB}: 0.38, N_{PCH}: 0.36

Figure 12. Assessment of the additional uncertainty on the DR value induced by the pressure variation in the loop by comparison of discrete data sets with a same power setting and inlet temperature. The reported pressure is that at the top of the loop, which is about 0.1 MPa lower than that at the bottom of the loop.

Figure 13. Assessment of the reproducibility of the DR values by comparison of two data series measured on different dates for the same inlet condition: T_{in} = -17°C.

Figure 14. Measurement qualification: A: no impact of the power steering frequency on the measured DR values; B: no impact of using the preheater on the measured DR values, T_{in}: -17°C

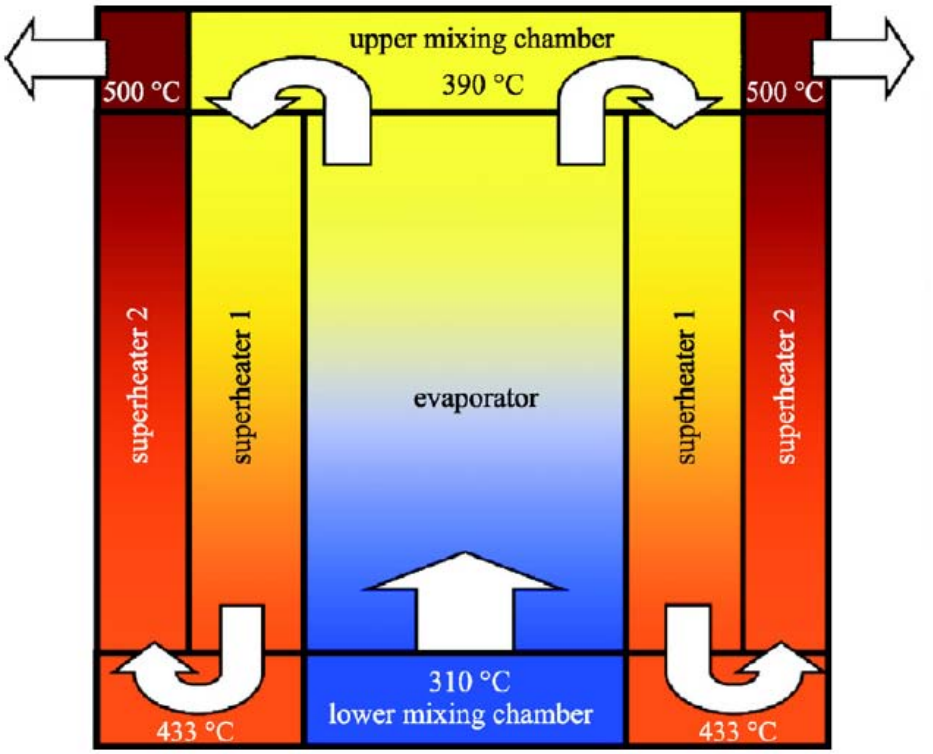

Figure 1. Schematic representation of the HPLWR, reproduced from Fischer et al.[5].

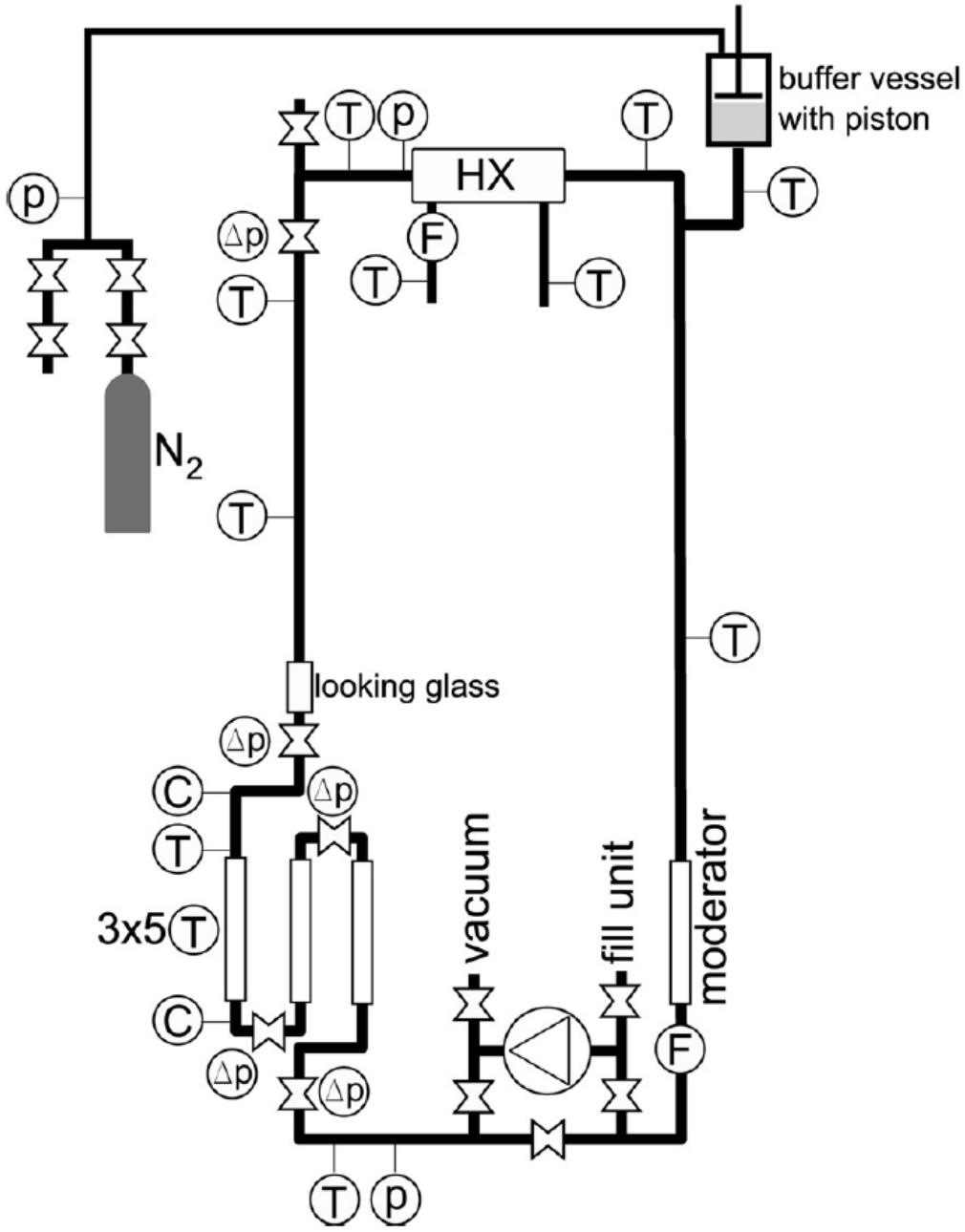

Figure 2. Schematic of the DeLight facility indicating the location of the different sensors.

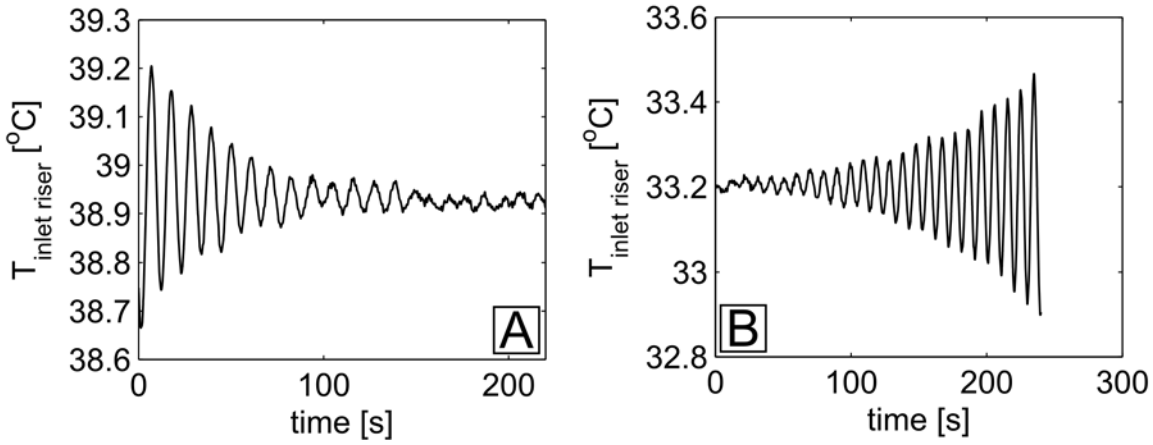

Figure 3. Examples of a stable (A) and unstable (B) temperature signal measured at the inlet of the riser section

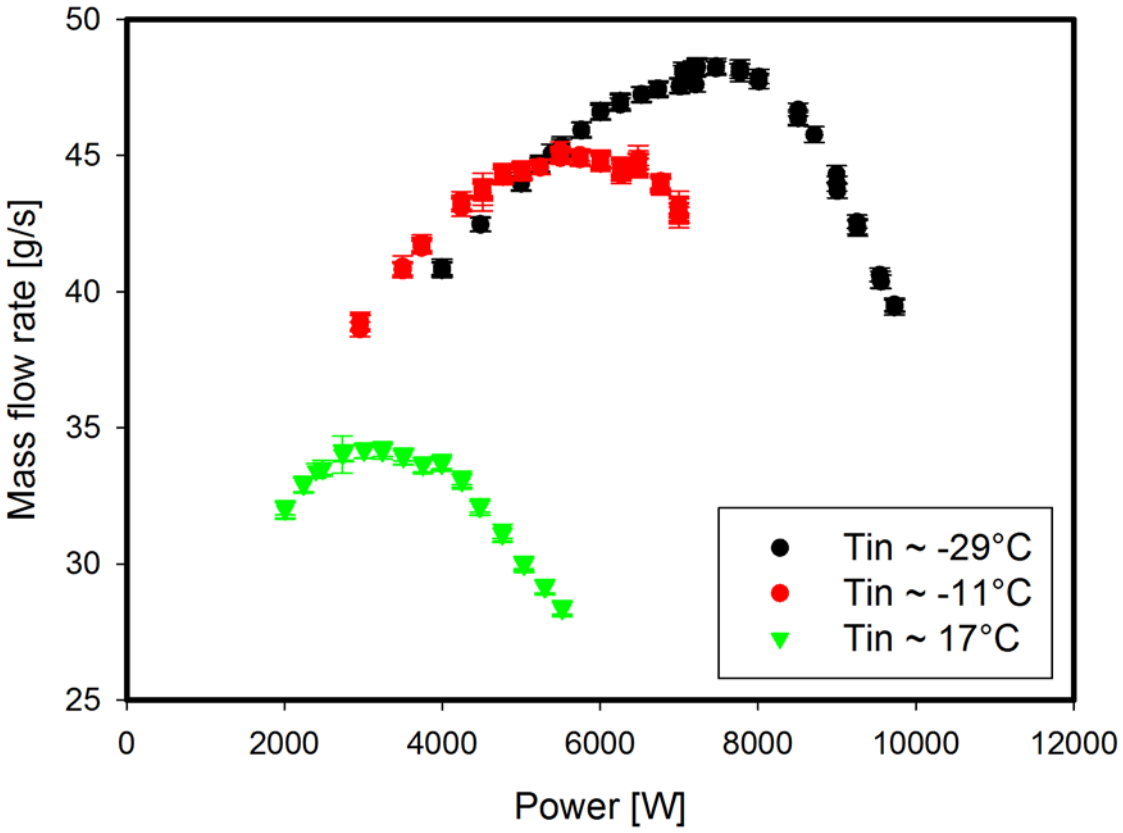

Figure 4: Measured power flow map data for a few selected inlet temperatures, R23 at 5.7 MPa.

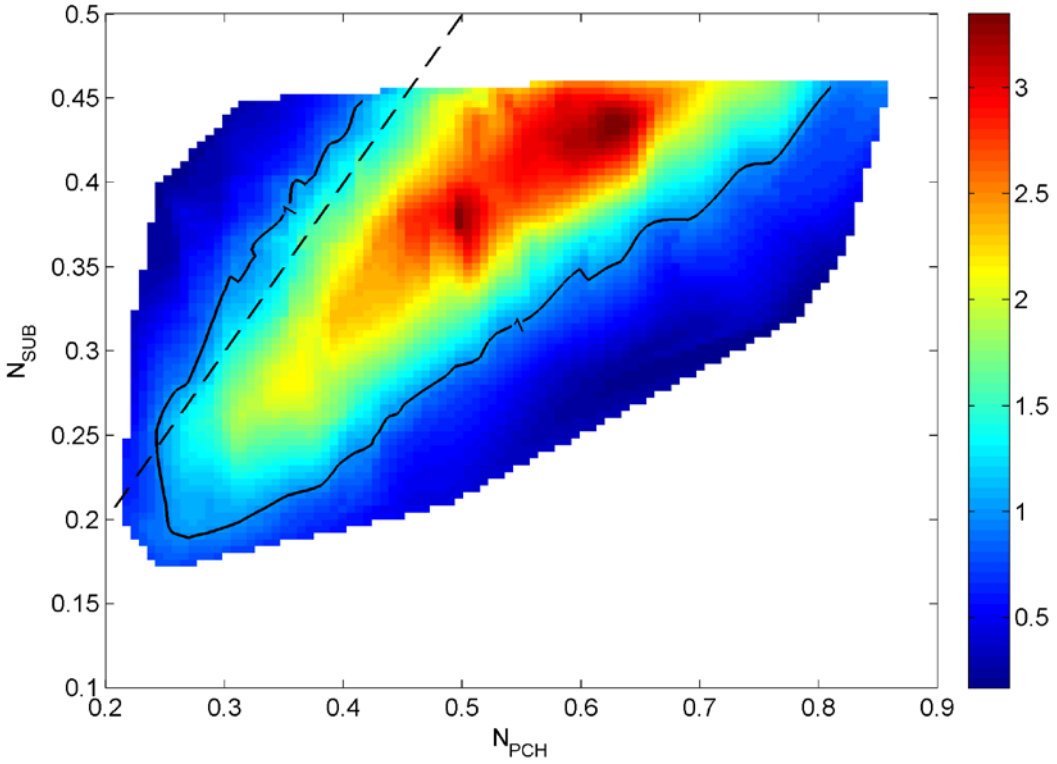

Figure 5. Contour plot of the measured DR values. The black line indicates DR = 1, the neutral stability line. The dashed line indicates where the exit temperature is equal to the pseudo-critical value.

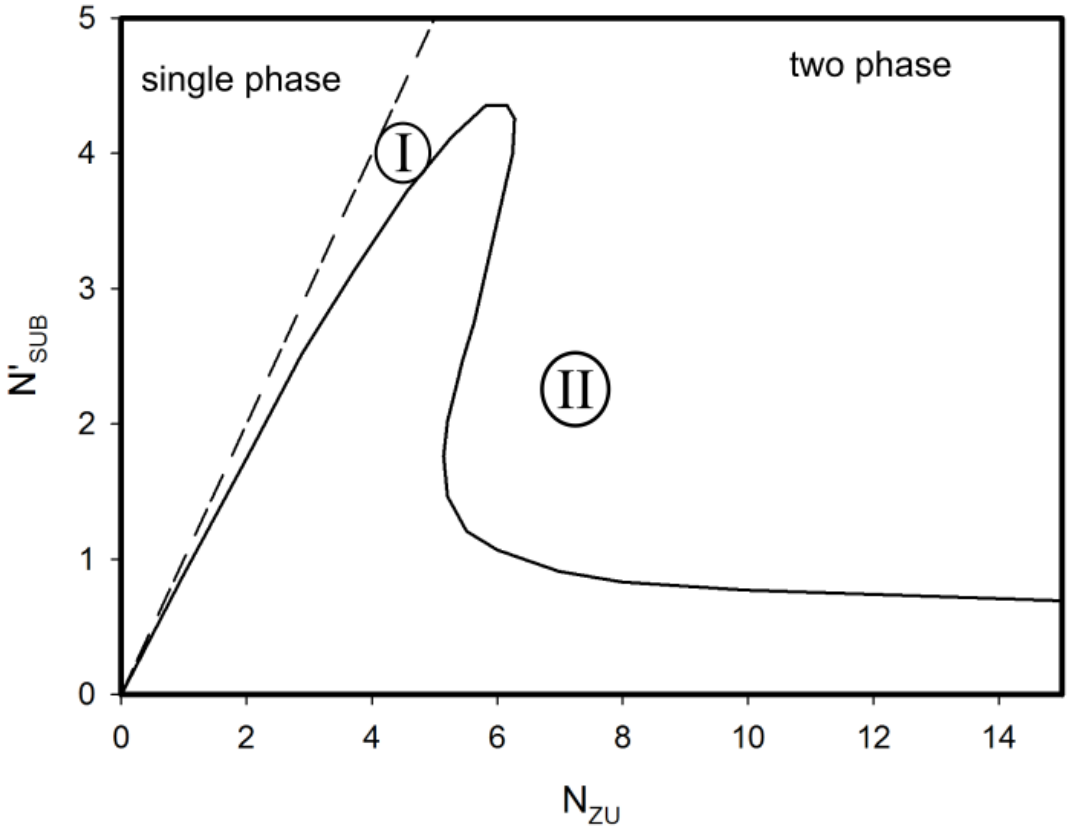

Figure 6. BWR stability plot, reproduced from Van Bragt and Van der Hagen [24].

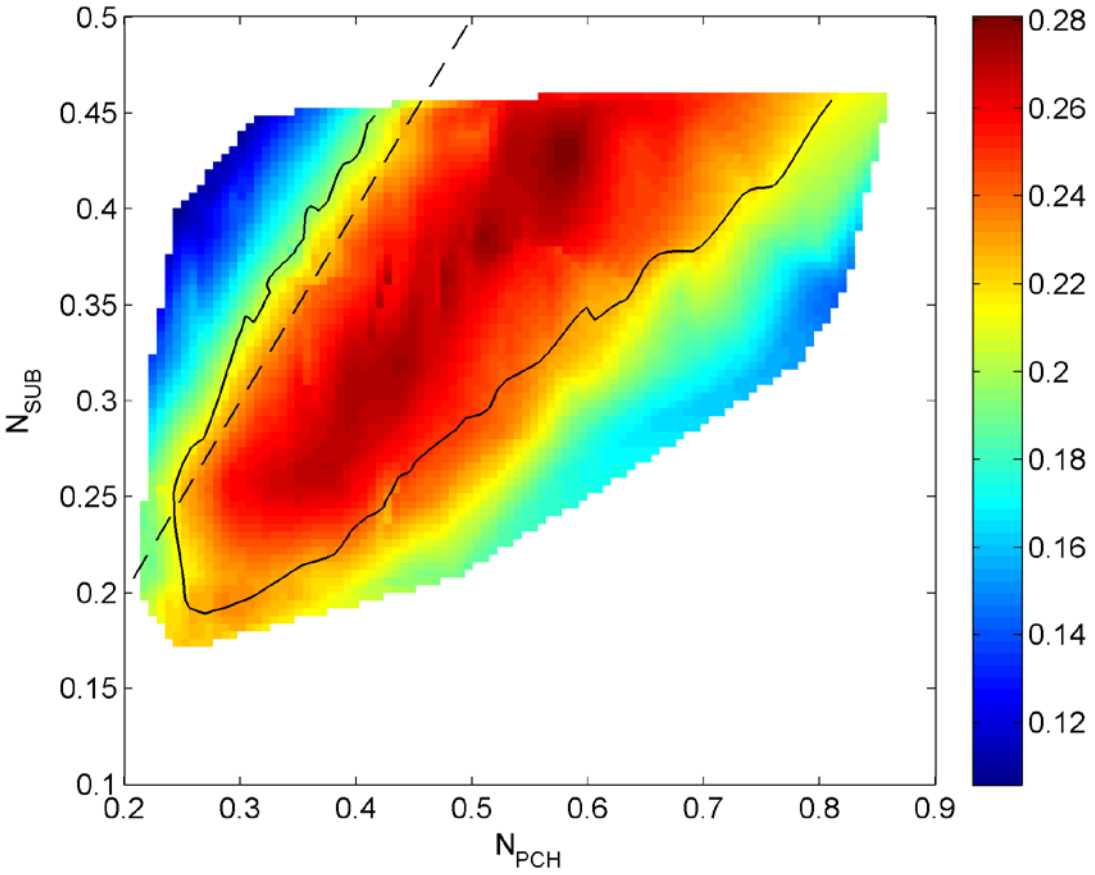

Figure 7. Contour plot of the measured frequencies. The black line indicates DR = 1, the neutral stability line. The dashed line indicates where the exit temperature is equal to the pseudo-critical value.

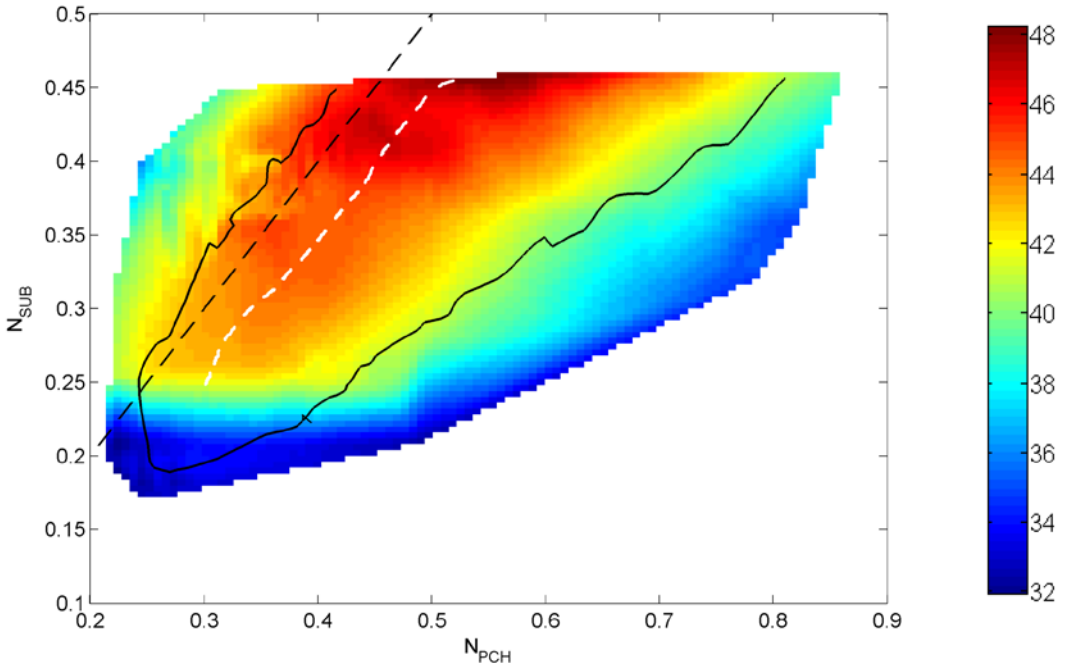

Figure 8. Contour plot of the measured mass flow rates (in g/s). The black line indicates DR = 1, the neutral stability line. The black dashed line indicates where the exit temperature is equal to the pseudo-critical value. The white dashed line qualitatively indicates the location of the maximum flow rate.

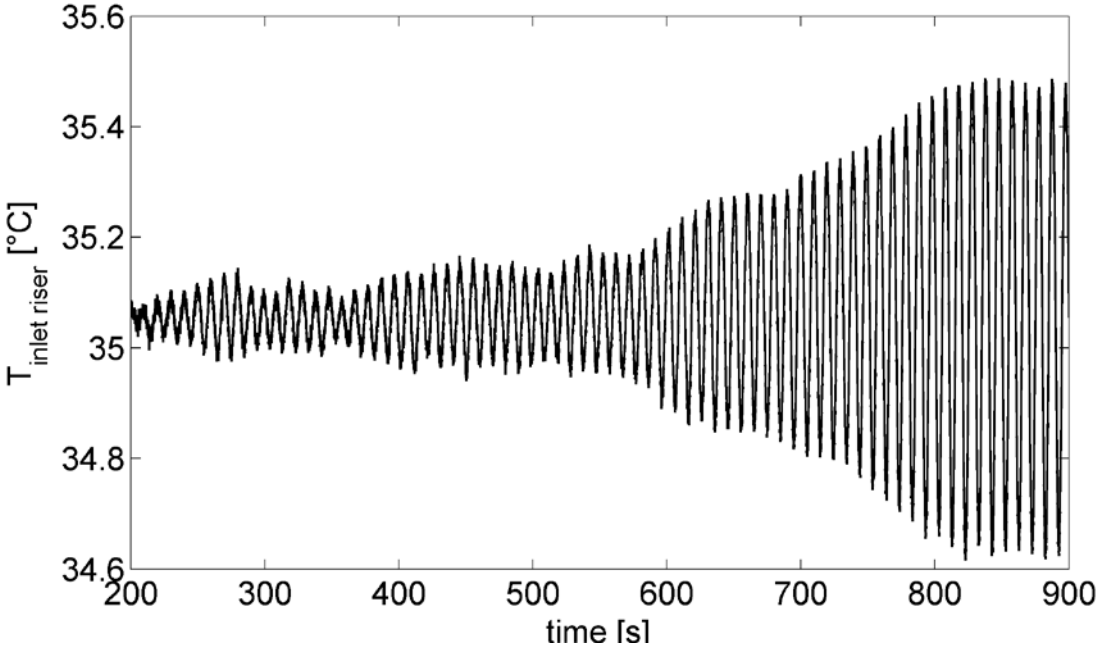

Figure 9. Illustration of non-linear effects which were recorded during the measurements: the occurrence of a limit cycle near the low power threshold.

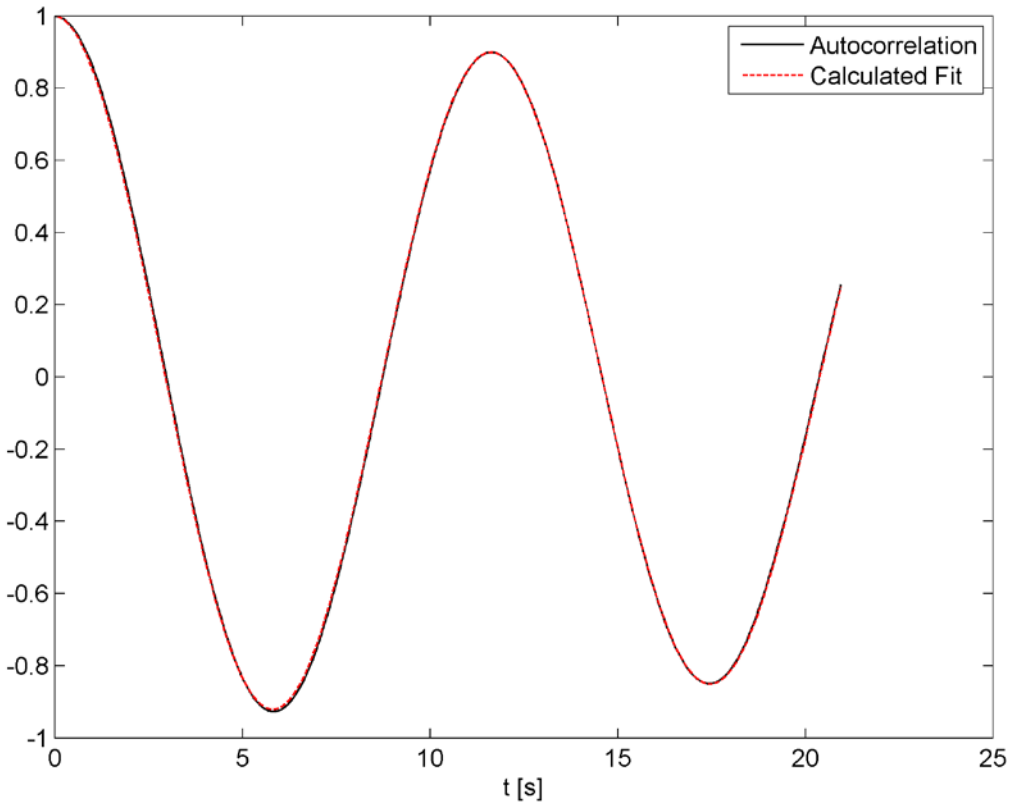

Fig. 10. Illustration of the fitted function and the autocorrelation of the measured temperature signal, N_{SUB}: 0.4, N_{PCH}: 0.37.

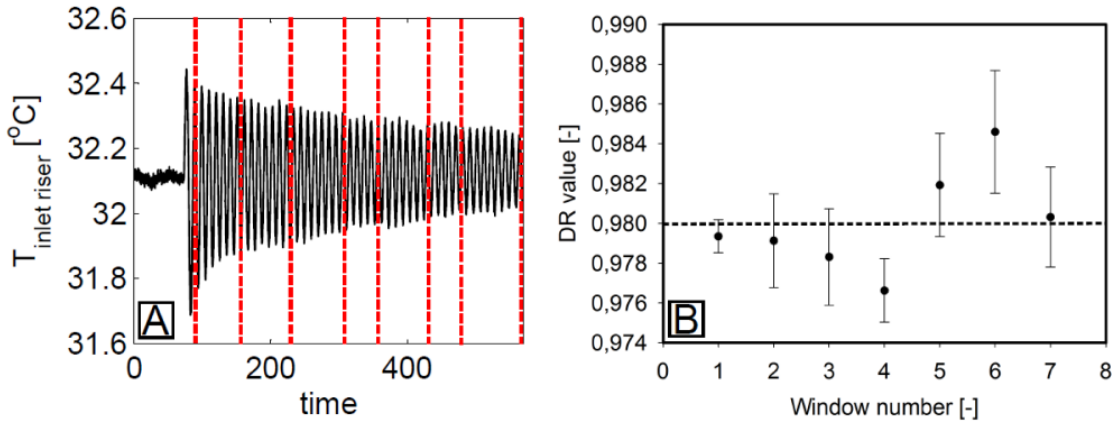

Figure 11. Verification of the fitting procedure to determine DR values. A: measured time signal and the selected windows, B: fitted DR values with their fitting uncertainty, N_{SUB}: 0.38, N_{PCH}: 0.36

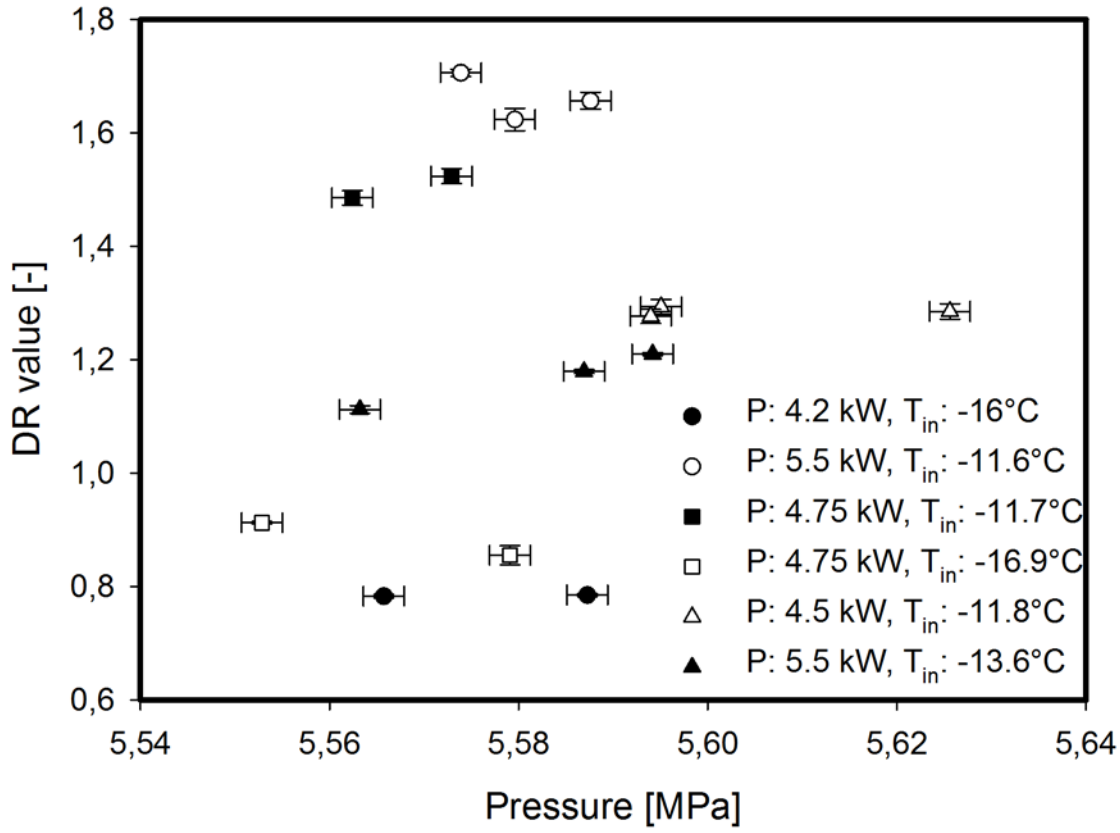

Figure 12. Assessment of the additional uncertainty on the DR value induced by the pressure variation in the loop by comparison of discrete data sets with a same power setting and inlet temperature. The reported pressure is that at the top of the loop, which is about 0.1 MPa lower than that at the bottom of the loop.

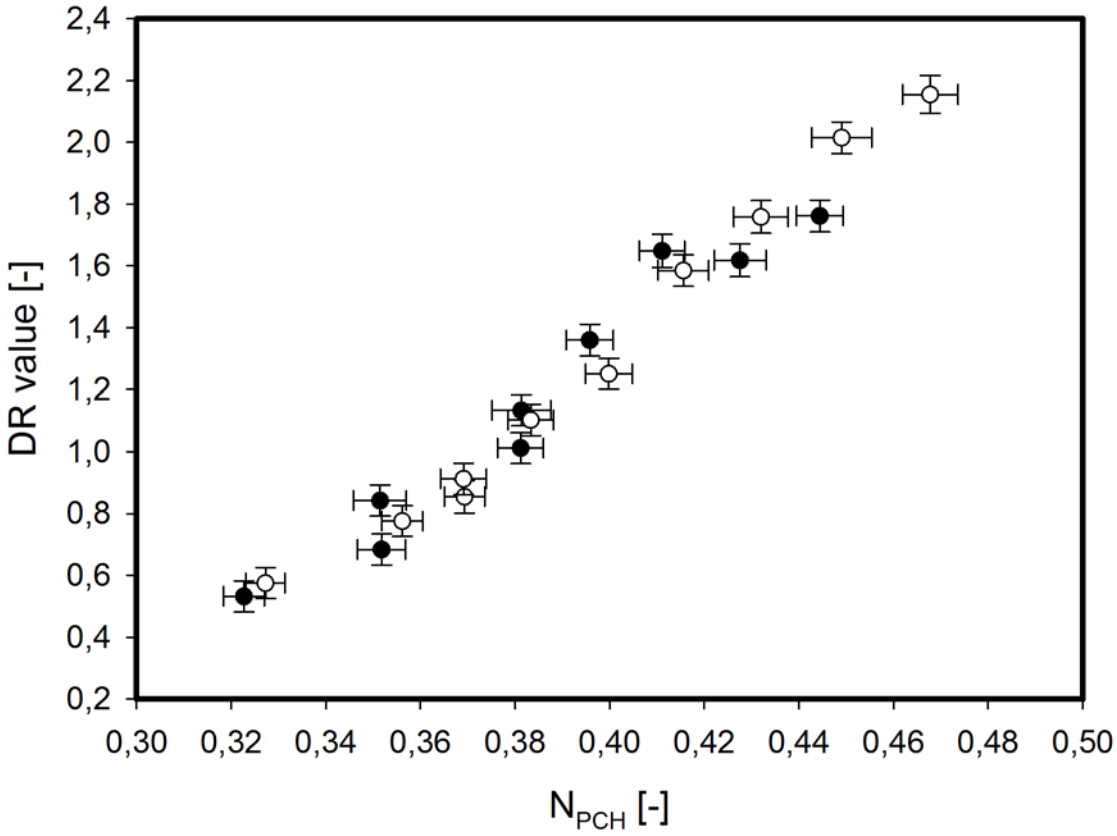

Figure 13. Assessment of the reproducibility of the DR values by comparison of two data series measured on different dates for the same inlet condition: T_{in} = -17°C.

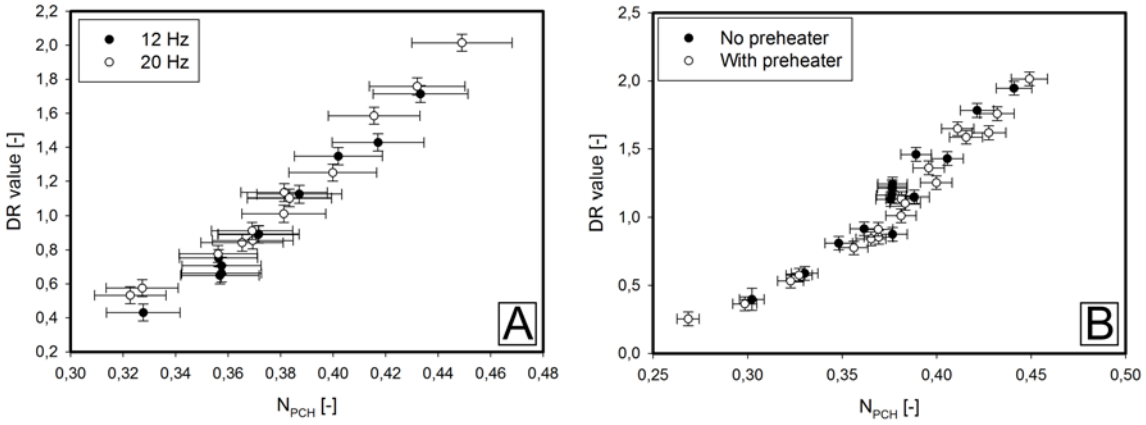

Figure 14. Measurement qualification: A: no impact of the power steering frequency on the measured DR values; B: no impact of using the preheater on the measured DR values, T_{in}: -17°C